Monthly Notices of the ROYAL ASTRONOMICAL SOCIETY

MNRAS **467,** 2367–2376 (2017)
Advance Access publication 2017 January 25

doi:10.1093/mnras/stx216

Trigonometric distance and proper motions of H_2O maser bowshocks in AFGL 5142

R. A. Burns,[1,2★] T. Handa,[2] H. Imai,[2] T. Nagayama,[3] T. Omodaka,[2] T. Hirota,[4,5] K. Motogi,[6] H. J. van Langevelde[1,7] and W. A. Baan[2,8]

[1]*Joint Institute for VLBI ERIC (JIVE), Postbus 2, NL-7990 AA Dwingeloo, the Netherlands*
[2]*Graduate School of Science and Engineering, Kagoshima University, 1-21-35 Kôrimoto, Kagoshima 890-0065, Japan*
[3]*Mizusawa VLBI Observatory, National Astronomical Observatory of Japan, 2-12 Hoshigaoka-cho, Mizusawa-ku, Oshu, Iwate 023-0861, Japan*
[4]*Mizusawa VLBI Observatory, National Astronomical Observatory of Japan, Osawa 2-21-1, Mitaka, Tokyo 181-8588, Japan*
[5]*Department of Astronomical Sciences, SOKENDAI, Osawa 2-21-1, Mitaka, Tokyo 181-8588, Japan*
[6]*Graduate School of Sciences and Technology for Innovation, Yamaguchi University,Yoshida 1677-1, Yamaguchi 753-8512, Japan*
[7]*Sterrewacht Leiden, Leiden University, Postbus 9513, NL-2300 RA Leiden, the Netherlands*
[8]*ASTRON, PO Box 2, NL-7990 AA Dwingeloo, the Netherlands*

Accepted 2017 January 23. Received 2017 January 20; in original form 2016 November 1

ABSTRACT

We present the results of multi-epoch VLBI (very long baseline interferometry) observations of water masers in the AGFL 5142 massive star-forming region. We measure an annual parallax of $\pi = 0.467 \pm 0.010$ mas, corresponding to a source distance of $D = 2.14^{+0.051}_{-0.049}$ kpc. Proper motion and line-of-sight velocities reveal the three-dimensional kinematics of masers in this region, most of which associate with millimetre sources from the literature. In particular, we find remarkable bipolar bowshocks expanding from the most massive member, AFGL 5142 MM1, which are used to investigate the physical properties of its protostellar jet. We attempt to link the known outflows in this region to possible progenitors by considering a precessing jet scenario and we discuss the episodic nature of ejections in AFGL 5142.

Key words: masers – stars: individual: AFGL 5142 – stars: massive – ISM: jets and outflows.

1 INTRODUCTION

Massive star formation is a challenging field of observational astronomy, with massive young stellar objects (MYSOs) residing in deeply embedded environments, often at great distances from Earth. From a theoretical perspective, high- and low-mass star formation were once considered distinctly different, with MYSOs initiating nuclear fusion while still deeply embedded in their parent cores, accretion persisting into the main sequence, in addition to producing strong radiation capable of limiting accretion on to the central star [see reviews by Zinnecker & Yorke (2007) and Tan et al. (2014)].

However, with recent advances in instrument sensitivity, resolution and data reduction techniques used in astronomy there has emerged a gradual convergence in the observed features present in low- and high-mass star formation. MYSOs are increasingly found to harbour disc–jet systems – a feature ubiquitous to low-mass star formation. Phenomena such as circumstellar discs (Beltrán et al. 2004; Hirota et al. 2014; Chen et al. 2016; Ilee et al. 2016), episodic ejection (Burns et al. 2016) and even jet rotation (Burns et al. 2015) are now becoming common targets of investigation in MYSOs.

In disc–jet systems, ejection rates correlate with accretion rates (Corcoran & Ray 1998; Caratti o Garatti et al. 2015) – thus the ejection history of an MYSO allows inference of its accretion history – which is itself unobservable in a practical sense due to the timescales involved. Accretion history, based on ejection history, can therefore be used to compare low- and high-mass star formation.

In addition to accretion mechanisms, outflows serve as another point of comparison – with the outflows of massive stars considered to be less collimated than those of low-mass stars (Wu et al. 2004). However, such conclusions are often based on surveys of large-scale outflows that could have formed via entrainment by a collimated, precessing jet as was observed in IRAS 20126+4104 (Shepherd et al. 2000). Evidently, all physical scales must be considered when comparing the outflows of low- and high-mass YSOs.

AFGL 5142 is a massive star-forming region that has multiple outflows on multiple scales. The region contains 9 millimeter cores, by far the most predominant of which being MM1 and MM2 which exhibit hot-core chemistry (Zhang et al. 2007; Palau et al. 2011, 2013). MM1 has a mass of about 6.5 $M_\odot$ (Liu et al. 2016) and houses an embedded massive star, indicated by the presence of 6.7-GHz methanol masers that trace an infalling disc (Goddi, Moscadelli & Sanna 2011). An ionized bipolar jet extends to the NW–SE – at an angle near perpendicular to the disc. Water masers tracing the leading tip of the ionized jet reveal expanding motions

★ E-mail: RossBurns88@googlemail.com

© 2017 The Authors
Published by Oxford University Press on behalf of the Royal Astronomical Society

Downloaded from https://academic.oup.com/mnras/article-abstract/467/2/2367/2957034 by ASTRON user on 29 November 2018

in the line of sight (l.o.s.) and sky-plane (Goddi & Moscadelli 2006; Goddi et al. 2011), thus giving AFGL 5142 MM1 the image of a prototypical disc–jet system in an MYSO. Furthermore, the combination of features associated with both low- and high-mass star formation make AFGL 5142 MM1 a good target for a comparative investigation.

About 1 arcsec to the South is MM2, with a mass of about 6.2 $M_\odot$ (Liu et al. 2016) but no centimetre emission or 6.7-GHz methanol masers. Both MM1 and MM2 exhibit similar hot molecular core chemical compositions (Zhang et al. 2007; Palau et al. 2011), suggesting similar evolutionary stages. Water masers have also been detected near AFGL 5142 MM2 (Hunter et al. 1995; Goddi & Moscadelli 2006).

Interferometric observations of the AFGL 5142 region in CO (2 − 1) (Zhang et al. 2007; Palau et al. 2011), SiO (2 − 1) and HCO^+ (1 − 0) (Hunter et al. 1999) reveal at least four distinct collimated molecular outflows on 10 arcsec scales; outflows A, B, C (Zhang et al. 2007) and outflow D (Palau et al. 2011). Several of these outflows intersect both MM1 and MM2, barring a simple assignment of progenitors. Single-dish observations reveal the presence of larger, arcmin scale outflows traced in CO (2 − 1) that also intersect the MM1 and MM2 regions (Hunter et al. 1995); these propagate primarily in the sky-plane. Recently Liu et al. (2016) also find a ∼9 arcsec length, extremely wide-angle bipolar outflow (EWBO), with an opening angle of ∼180°, driven from the MM1 to MM2 region, leading the authors to interpret its formation as being driven by a precessing jet rather than entrainment at wide angles from a narrow jet.

In this work, we investigate the outflows seen in AFGL 5142 at the smallest scales by performing new multi-epoch very long baseline interferometry (VLBI) observations of water masers at 22-GHz. VLBI is an ideal observational approach to investigating protostellar ejections as multi-epoch observations provide sky-plane and l.o.s. information, thus revealing the three-dimensional (3D) kinematics of gas in the vicinity of MYSOs. Our investigation aims to provide observational characterization of outflow behaviour (launching mechanisms and episodic ejection) for a prototypical MYSO and to provide comparison between low- and high-mass formation mechanisms. Our report concentrates on the kinematics and energetics of the jets associated with AFLG 5142 MM1. We use our findings to offer a reinterpretation of the recent history of jets and outflows in this region and attempt to assign progenitors to each of the known outflows from the literature. Via annual parallax, we also provide the first precise measurement of the distance to AFGL 5142; a quantity essential for converting observations to physical quantities such as ejection velocities, ages and momentum rates.

2 OBSERVATIONS AND DATA REDUCTION

VLBI observations of AFGL 5142 were carried out with VLBI exploration of radio astrometry (VERA), the observing calendar is detailed in Table 1. All observations were conducted in dual-beam mode (Kawaguchi, Sasao & Manabe 2000) with beams centred on the maser target, AFGL 5142 and a reference quasar, J0533+3451. For both beams, left-hand circular polarization signals were recorded at each of the four VERA stations. Data were collected and correlated using the Mitaka FX correlator (Chikada et al. 1991), adopting a rest frequency of 22.235080 GHz. For AFGL 5142 data, we used a phase tracking centre of $(\alpha, \delta)_{J2000.0} = (05^h30^m48\overset{s}{.}01733742, +33°47'54\overset{''}{.}56750)$ and for J0533+3451 data we set a phase tracking centre at $(\alpha, \delta)_{J2000.0} = (05^h33^m12\overset{s}{.}76510600, +34°51'30\overset{''}{.}336995)$. Further phase corrections, including more accurate atmospheric models and antenna positions than those used at correlation, were made and applied post-calibration.

Table 1. Summary of observations.

Epoch number	Observation date	Modified Julian date	Number of features
1	2014 April 21	56768	12
2	2014 May 20	56797	9
3	2014 October 2	56932	17
4	2014 November 25	56986	22
5	2015 January 31	57053	24
6	2015 March 29	57110	25
7	2015 May 29	57171	19

The total correlator bandwidth of 240 MHz was shared into 16 intermediate frequencies (IFs). One IF was allocated to the maser data with a bandwidth of 8 MHz and 15.63 kHz channel spacing, providing a 0.12 km s^{-1} velocity spacing. The remaining 15 IFs were allocated to the data of the quasar reference source – one IF had similar properties to the maser data, while the other 14 IFs had 16 MHz bandwidth and spacings of 125 kHz. The 15 quasar data IFs were manipulated into common form and merged, resulting in almost continuous frequency coverage spanning 232 MHz.

Data reduction was performed using Astronomical Image Processing System (AIPS), developed by National Radio Astronomy Observatory. VLBI phase referencing data reduction made use of the *inverse phase referencing* technique, customised for the dual-beam data of VERA. The technique was first introduced in Imai et al. (2012) and further development, in addition to a guide to its implementation, is given in Burns et al. (2015).

In short, data reduction involves solving frequency-dependant phase terms (group delay) using bright calibrators in the wider 15 IF data set, while time-dependant phase terms are solved using the narrow but bright line emission of the maser. Both sets of solutions are then applied to the reference source, J0533+3451, inversely giving the angular separation of the maser from the phase centre. Assuming that the reference source is fixed at its ICRF coordinates, we then obtain the astrometric position of the maser from the derived separations. Since phase solutions determined using the maser are applied to itself, we also produce high-quality, astrometrically accurate maser maps. Typically, maser maps achieved rms noise values of 100–200 mJy beam^{-1}, while the wider band continuum data achieved typical rms values of ∼1 mJy.

Maser maps were produced using the AIPS task CLEAN in automatic mode (DOTV = 0), with a synthesized beam of dimensions 1.0 × 1.2 mas. Masers were identified from the maps using an automated *SAD* routine in AIPS, employing a detection signal-to-noise cut-off of 7. Following common nomenclature, a 'spot' refers to an individual maser emission peak, imaged in a single spectral channel, while a maser 'feature' refers to a collection of spots considered to emanate from the same physical maser cloud. Maser spots were grouped into a feature if they shared a spectral feature and collocated within a radius of 1 mas. The associations of spots to features, and the flux weighted astrometric positions of maser features, were determined using a basic FORTRAN code that also removes the offset introduced by the difference in coordinates between the phase tracking centre and the reference maser used in each epoch, in addition to shifting the maser maps to the absolute reference frame.

Downloaded from https://academic.oup.com/mnras/article-abstract/467/2/2367/2957034 by ASTRON user on 29 November 2018

3 RESULTS

3.1 Maser distribution and l.o.s. velocities

A total of 27 independent maser features were detected with VERA during the observing calendar. Their coordinates, l.o.s. velocities, detection frequencies and other properties are recorded in Table 2. With regard to temporal variability, some maser features persisted through all epochs, while others exhibited more sporadic behaviour. No periodic behaviour was noted. Fig. 1 shows the temporal changes in the overall emission spectrum, and the variability of individual maser features can be read from the detection frequencies in column 3 of Table 2. The distributions of all maser features detected by VERA are shown in Fig. 2.

Fig. 3 shows a magnified view of the MM1 region. Masers trace three arc structures contained in a region of about 300 × 300 mas. There exists one maser arc to the North-West of the system centre, and two proximate and similarly oriented arcs lying to the South-East, one closer and one further from the system centre. We refer to these as the 'NW', the 'SE inner', and 'SE outer' maser arcs, respectively – and are hence categorised accordingly in column 1 of Table 2. The NW masers arcs are redshifted and the SE masers are blueshifted with respect to the l.o.s velocity of the region (-1.1 km s^{-1}; Zhang et al. 2007).

Maser feature A (see Table 2) is also associated with MM1. This maser does not associate with the aforementioned arcs, and rather, stands in the midway – near the system centre, at map position $(\alpha, \delta) = (7, -41)$ mas. This maser exhibits some remarkable properties that will be discussed in a later publication.

Our observations did not detect all of the masers reported by Goddi & Moscadelli (2006). In their VLBA observations, they find

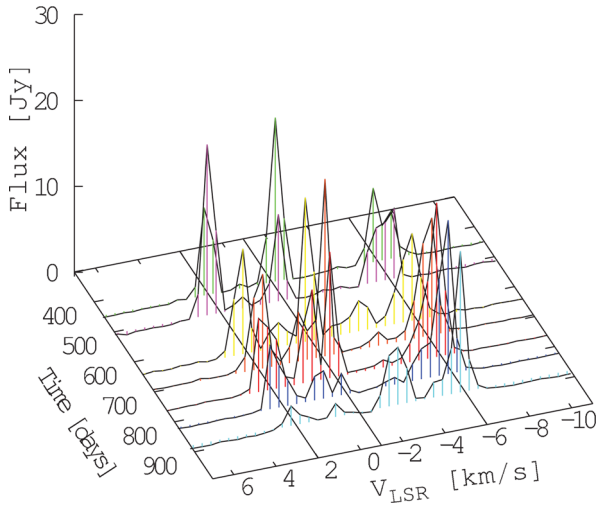

Figure 1. Scalar averaged cross-power spectra of the maser emission in AFGL 5142 as a function of time, coloured arbitrarily.

Table 2. The general properties of H_2O masers in AFGL 5142, detected with VERA.

Maser ID	V_{LSR} (km s^{-1})	Detected epochs	$\Delta\alpha\cos\delta$ (mas)	$\Delta\delta$ (mas)	$\mu_\alpha\cos\delta$ (mas yr^{-1})	μ_δ (mas yr^{-1})	F_{int} (Jy)	π (mas)
NW1	2.47	1234567	−35.216	35.133	−0.55 ± 0.03	0.89 ± 0.26	23.67	0.460 ± 0.014
NW2	0.42	1234567	−39.637	29.447	−1.03 ± 0.02	0.23 ± 0.11	11.09	0.479 ± 0.021
NW3	3.49	****567	−28.365	38.437	0.07 ± 0.27	0.16 ± 0.05	1.27	–
NW4	3.07	1*34*67	−37.371	32.979	−0.58 ± 0.08	1.07 ± 0.08	2.99	–
NW5	1.81	**34567	−38.121	31.934	−0.19 ± 0.48	1.51 ± 0.80	4.13	–
NW6	1.24	****567	−38.838	30.803	−1.28 ± 0.06	−0.21 ± 0.11	4.14	–
NW7	0.86	**3*567	−41.625	24.954	−0.77 ± 0.12	0.87 ± 0.31	2.22	–
NW8	−0.02	****567	−45.198	19.198	−0.73 ± 0.42	1.98 ± 0.21	2.46	–
SE1	−6.69	123456*	162.415	−232.163	1.13 ± 0.14	−1.59 ± 0.04	4.83	–
SE2	−6.20	1234567	156.283	−237.916	1.93 ± 0.03	−1.16 ± 0.03	12.87	0.479 ± 0.022
SE3	−6.71	1**4567	147.805	−222.823	1.38 ± 0.19	−0.83 ± 0.11	1.77	–
SE4	−4.93	**34567	134.663	−228.13	0.84 ± 0.04	−1.19 ± 0.08	5.31	–
SE5	−5.36	***4567	117.507	−230.753	0.36 ± 0.04	−1.08 ± 0.02	2.72	–
SE6	−6.91	****567	160.06	−235.217	1.97 ± 0.70	−1.67 ± 0.26	2.52	–
SE7	−4.08	**3****	121.616	−227.994	–	–	1.41	–
SE8	−7.05	*****6*	131.305	−229.803	–	–	5.80	–
SE9	−7.05	*****6*	159.065	−236.213	–	–	0.88	–
SE10	−5.77	**3****	54.856	−143.514	–	–	2.15	–
FS1	−5.78	1234567	11.783	−1241.213	1.42 ± 0.03	−0.43 ± 0.07	13.98	0.450 ± 0.029
FS2	−4.41	***4567	12.405	−1227.991	1.64 ± 0.08	0.05 ± 0.21	17.80	–
FS3	−5.15	123456*	13.319	−1236.244	– 1.71 ± 0.04	0.71 ± 0.18	5.74	–
FS4	−4.43	**34567	13.227	−1230.149	1.35 ± 0.08	1.00 ± 0.11	4.67	–
FS5	−5.54	1234567	11.416	−1225.99	1.13 ± 0.09	1.44 ± 0.23	11.02	–
B	0.77	1*3456*	639.914	148.019	1.89 ± 0.06	−0.61 ± 0.04	3.06	–
FSW	−3.04	**3456*	−3457.993	−1553.682	−2.56 ± −0.46	0.01 ± 0.18	3.29	–
A	−3.18	123456*	6.68	−40.77	–	–	1.27	–
							Simultaneous fit	0.467 ± 0.010

Notes. Column (2): L.o.s. velocities, with respect to the local standard of rest, are quoted as those measured for the first detection.
Column (3): Numbers indicate detection in the corresponding epoch, while asterisk represents non-detection.
Column (8): Integrated fluxes are given as the average of measurements from all epochs.

Downloaded from https://academic.oup.com/mnras/article-abstract/467/2/2367/2957034 by ASTRON user on 29 November 2018

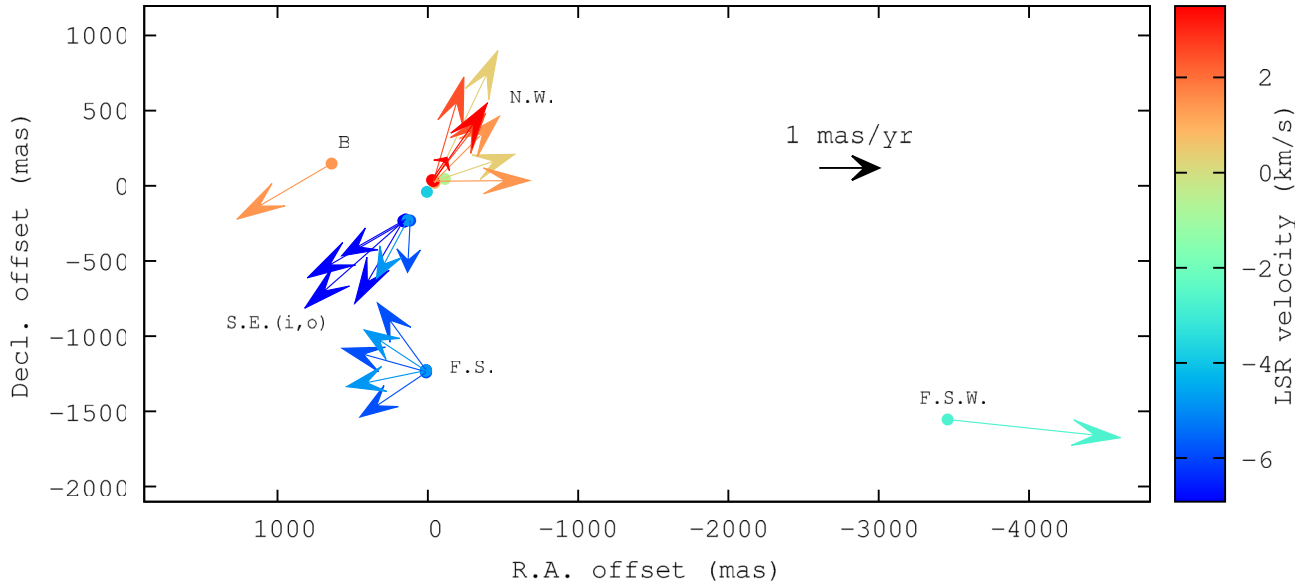

Figure 2. Internal motions of water masers in AFGL 5142. Vector magnitudes indicate proper motion, while colours indicate LSR velocity. Annotations are the same as those in Table 2, with SEi and SEo referring to the 'inner' and 'outer' South-East groups, respectively. The map origin is at the phase tracing centre of the maser data.

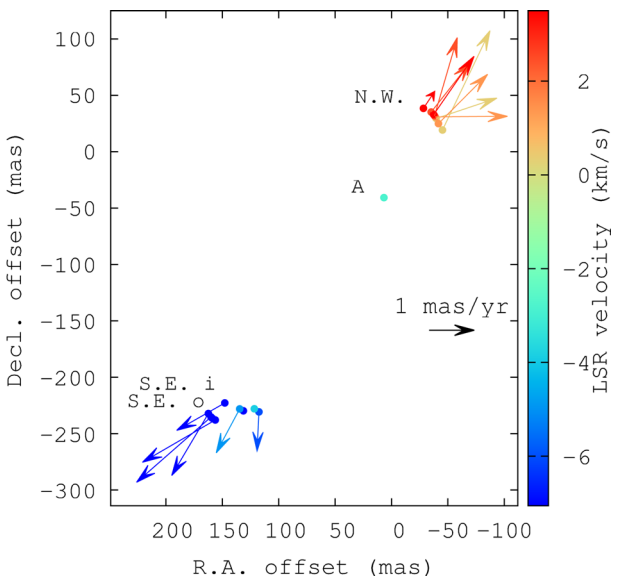

Figure 3. Same as Fig. 2 for the MM1 core region.

more water masers associated with MM1 that are located further to the NW. We include their results in our investigation of the maser distribution in AFGL 5142 MM1 (see Section 3.4).

Water masers associated with MM2 are arranged in a single arc (see Fig. A2). Due to their location 'far South' of the phase tracking centre, we refer to these masers as the FS group in Table 2. These masers likely correspond to maser features 'IIb' of Goddi & Moscadelli (2006). All FS masers have slightly blueshifted l.o.s. velocities.

We found one maser to the North-East ('B' in Table 2) of the phase tracking centre – possibly associated with MM1 and probably corresponding to maser feature 'IIr' of Goddi & Moscadelli (2006). One maser feature was found in the far South-West (FSW), associated with AFGL 5142 MM6.

3.2 Fitting parallax and proper motion

The astrometry of water masers observed with VERA was used to measure the annual parallax and resulting trigonometric distance of the AFGL 5142 region. To assure the best possible precision for the distance estimate, we performed parallax fitting only using maser features that were detected in all seven epochs – spanning just over 1 yr. Four maser features passed this criterion, two of which were in the NW bowshock, one in the SE bowshock and one in the FS bowshock. Parallax fitting was done simultaneously for the four maser features, assuming a common distance, to average and smooth out noise-like and structure-induced errors. Additional error floors were added and reduced iteratively until a χ^2 value of unity was reached. Required error floors were 0.04 and 0.27 mas in RA and Dec., respectively.

We estimate the annual parallax of AFGL 5124 to be $\pi = 0.467 \pm 0.010$ mas, corresponding to a trigonometric distance of $D = 2.14^{+0.051}_{-0.049}$ kpc, firmly placing it in the Perseus Arm. Fits are shown in Fig. 4. To confirm the reliability of our simultaneous fitting, the parallaxes (see Table 2: column 9) and proper motions of each of the four maser features were then fit independently and were found to be consistent with each other and with the simultaneous fit. Note that our consistent distances to MM1 and MM2 confirm that they are in close physical proximity.

Using feature NW1 as reference, we obtained the relative proper motions of all other maser features that were detected in at least three epochs, of which there were 21. These relative motions were then converted to absolute proper motions (see Table 2, columns 6 and 7) using the absolute proper motion of feature NW1 from the astrometric fitting procedure described earlier. Proper motion errors were calculated as the quadrature sum of the standard deviation in the relative proper motion and the proper motion uncertainty of feature NW1.

3.3 Systemic motion and internal motions

Absolute (observed) proper motions are a composition of the internal motions of masers in the frame of the driving source, and the

Downloaded from https://academic.oup.com/mnras/article-abstract/467/2/2367/2957034 by ASTRON user on 29 November 2018

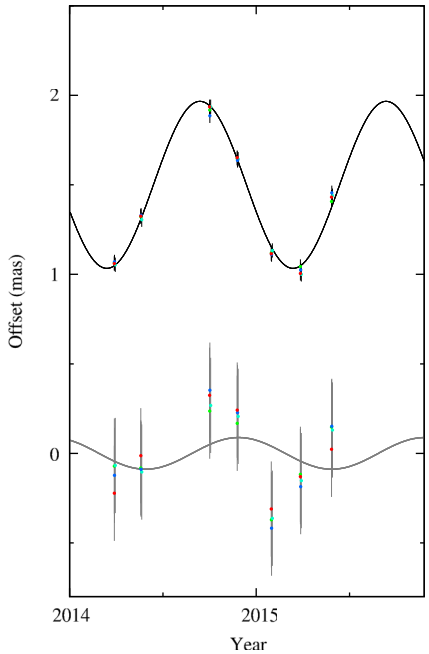

Figure 4. Annual parallax motions of four maser features in AFGL 5142 in (above) RA and (below) Dec. directions. Maser features are coloured arbitrarily and error floors are represented by vertical bars.

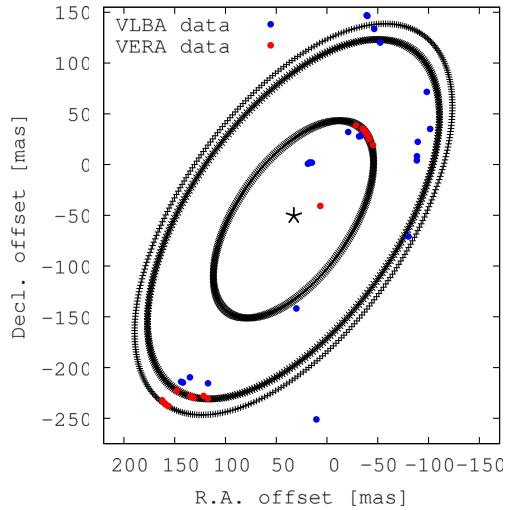

Figure 5. Ellipses fit to the VERA data, assuming a common origin and independent ejections for NW, SEi and SEo masers. VLBA data from 2004 (Goddi & Moscadelli 2006) are also shown.

apparent systemic motion of the source across the sky as governed by Galactic dynamics. In the case where a source's internal motions are expected to be symmetric, the sum of all motion vectors should balance to zero – the systemic proper motion of the region is derived from the residual of this summation. In AFGL 5124, we used the proper motions of masers associated with the NW and SE maser bowshocks in MM1 (eight and six maser features, respectively), since the masers in this region are known to trace a symmetric bipolar ejection (Goddi et al. 2007). The resulting systemic motion was $(\mu_\alpha \cos\delta,\ \mu_\delta) = (+0.32 \pm 0.27,\ -0.22 \pm 0.47)$ mas yr^{-1}, where errors were calculated as the quadrature sum of the average errors of all maser motions in each bowshock.

Subtracting the systemic proper motion from all absolute proper motions reveals the internal motions in the frame of the driving source, these are shown in Figs 2 and 3.

Masers in MM1 trace arc shaped shocks that are expanding from the centre of the system at an average velocity of 15 km s^{-1}. We interpret these as bowshocks tracing the protostellar jet reported by Goddi & Moscadelli (2006) and Goddi et al. (2011) and discuss these in further detail later. The masers associated with MM2 also appear to trace an expanding arc. However, the detection of only Easterly propagating components, i.e. without a symmetric counterpart in the West, precludes detailed analysis of its kinematics.

Maser feature A could not be assigned a proper motion, since its motion in the sky-plane was strongly non-linear.

3.4 Single versus episodic ejection

To investigate the physical nature of ejections from MM1, we performed least-squares fitting of elliptical jet shells to the maser distributions to evaluate their morphology and to determine the centre position of the system. Since our maser data reveal two independent bowshocks in the SE lobe, we must consider that ejections may occur in multiple episodes rather than a single ejection event; thus, ellipses were fit under the condition that the three ejections, each traced by a bowshock, originate from a common centre. We find that the data are best fit to concentric ellipses with an origin at $(\alpha, \delta) = (33, -54)$ mas, shown as a star in Fig. 5. The centre position coincides with the methanol disc reported by Goddi et al. (2007) and is near to maser feature A that exhibits non-linear motions (see Section 4.1.5). The physical distances of the bowshocks from the system centre were 240, 437 and 475 AU for the NW, SE inner and SE outer masers, respectively, assuming that these bowshocks are close the plane of the sky. The shocked surfaces extend about ∼50 AU in a direction perpendicular to the outflow direction, indicating a high degree of collimation.

The difference in the ejection radii of the NW and SE bowshocks groups in our model can be interpreted either as separate asynchronous ejections expanding from the centre at constant velocity, or as a quasi-single ejection event with non-equal propagation velocities – possibly due to a density gradient in the vicinity of the YSO. The former interpretation appears favoured, considering the results of Goddi & Moscadelli (2006) who find masers further in the NW direction than those observed with VERA (Fig. 5). These masers align well with the ellipses fit to the VERA data (even though the VLBA data were not used for fitting) and may thus be counterparts to the SE bowshocks.

Assuming expansion at constant velocity the ages of ejection events – i.e. the time it would have taken for ejecta to reach the positions of the observed bowshocks – can be estimated from their distance from the star divided by their outward motion. We measured average internal motions of 1.4 mas yr^{-1} for each of the lobes in opposite directions. For the ejections observed in AFGL 5142 MM1, we estimate ejection ages of 80, 145 and 159 yr for the NW, SE inner and SE outer bowshocks, respectively. In this scenario, the SE bowshocks would be roughly twice the age of the NW bowshock, with 14-yr interval between the ejections of the SE inner and SE outer ejections.

Downloaded from https://academic.oup.com/mnras/article-abstract/467/2/2367/2957034 by ASTRON user on 29 November 2018

4 DISCUSSION

4.1 Physical properties of the jet

4.1.1 Outflow driving mechanism

Masers in AFGL 5142 MM1 trace arcs of shocked gas at the leading edge of a protostellar jet. Using the proper motions of masers measured with VLBI, we can investigate the physical properties of the jet by comparison with published outflow models. VLBI maser data are well suited for comparison with the models of Lee et al. (2001) and Ostriker et al. (2001) who describe the motions of gas in the shocked region between a protostellar outflow and the ambient gas. In their works, they compare two models; a jet-driven bowshock and a stellar wind. Generally, the prevalence of each model can be determined by the amount of transverse motion observed near the head of the jet; in a jet-driven outflow, the transverse velocity is large as the jet material disperses at the bowshock, while the transverse velocities in a stellar wind tend to zero at the tip since in a momentum-driven stellar wind the gas propagates radially outward from the YSO and thermal pressure is negligible.

Using a jet position angle of -35°, we measure transverse proper motions in a velocity range of 0–13 km s^{-1}, with a mean value of 4 km s^{-1}. The large range of transverse motions indicates that the outflow in AFGL 5142 MM1 is dominated by jet-driven bowshock kinematics. Since masers in AFGL 5142 MM1 exclusively trace the leading surface of the outflow, it is difficult to quantify any contribution from a stellar wind – whose influence is more easily seen along the body of the outflow. Other similar works comparing VLBI determined maser proper motions with the models of Lee et al. (2001) and Ostriker et al. (2001) also find MYSO jets to be dominated by jet-driven bowshocks with some contribution from a lower velocity wind (Sanna et al. 2012; Burns et al. 2016).

4.1.2 Jet momentum rate

In addition to investigating the driving mechanism, we can calculate the momentum rate (force) of the jet via the expression used by Goddi et al. (2011):

$$\dot{P}_{\rm outflow} = 1.5 \times 10^{-3} V_{10}^2 R_{100}^2 (\Omega/4\pi) n_8 [{\rm M}_\odot\ {\rm km\,s^{-1}\ yr^{-1}}], \qquad (1)$$

where V_{10} is the maser velocity in units of 10 km s^{-1}, R_{100} is the radial distance of the masers from the driving source in units of 100 AU, Ω is the opening solid angle of the jet and n_8 is the volume density of ambient gas in units of 10^8 cm^{-3}. The following parameters used in the calculation were derived from our observations of the NW maser bowshock: $v = 14$ km s^{-1}, $R = 240$ AU and SE bowshock: $v = 14$ km s^{-1}, $R = 475$ AU. Furthermore, we take $\Omega = 1.1$ sr from the jet continuum observations of Goddi et al. (2011). Regarding the ambient density, n_8, we consider values in the range of 10^7–10^9 cm^{-3}, which are simulated initial ambient densities suitable for producing masers in shocks (Kaufman & Neufeld 1996). We arrive at a range of momentum rates between $\dot{P} = 10^{-4}$ and 10^{-2} M$_\odot$ km s^{-1} yr^{-1} for both bowshocks. These ranges are consistent with Goddi et al. (2011) and the extended molecular outflows in AFGL 5142 MM1 (see Table 3).

If we instead derive the jet opening angle directly from the maser data, we arrive at $\Omega = 0.07$ sr and momentum rate ranges of $\dot{P} = 10^{-6}$–10^{-4} M$_\odot$ km s^{-1} yr^{-1}. The fundamental property that maser emission arises in regions of special physical conditions and that they are observed preferentially along surfaces tangential to the observer can complicate maser-derived estimates of the jet opening angle – except for cases where the jet head and body are more fully traced. As such, we argue that the jet opening angle derived from the continuum observations of Goddi et al. (2011) is preferred.

Table 3. Outflow parameters from this work and the literature.

Tracer	Length (arcsec)	PA (°)	Momentum rate (M$_\odot$ km s^{-1} yr^{-1})	Notes
CO (2 − 1)	40	34	1.11×10^{-4}	1
HCO$^+$ (1 − 0)	–	–	4.52×10^{-3}	2
SiO (2 − 1)	30	10	–	2
CO (2 − 1)	30	5	2.85×10^{-3}	'Outflow A', 3
CO (2 − 1)	10	−40	2.38×10^{-3}	'Outflow C', 3, 4
H_2O ($6_{16} - 5_{23}$)	0.1	−35	10^{-4}–10^{-2}	This work

Notes. Column (5): 1 – Hunter et al. (1995); 2 – Hunter et al. (1999); 3 – Zhang et al. (2007); 4 – Palau et al. (2011).

4.1.3 Primary jet velocity

When the ram pressure of the jet is sufficient to balance that of the swept up material, the relationship between the velocities of the primary jet and that of the swept up gas is given as $v_j \approx v_{ws}(1 + \sqrt{n/n_j})$, adapted from Chernin et al. (1994), where v_j and v_{ws} are the velocities of the primary jet and working surface (traced by the bowshock velocity), and n and n_j are the ambient and jet number densities, respectively. For the ambient density, we use $n = 10^8$ cm^{-1}, adopted from shock models Hollenbach, Elitzur & McKee (2013). Regarding the jet density, n_j, Caratti o Garatti et al. (2015) find primary jet electron densities of $n_e \sim 10^3$–10^4 cm^{-3} in their survey of MYSOs. Employing an ionization fraction of $x_e = n_e/n_H = 0.1$ (Hartigan, Morse & Raymond 1994), the MYSO primary jet densities fall in the range of $n = 10^4$–10^5 cm^{-3}. Finally, we estimate primary jet velocities in the range of $v_j \sim 100$–1000 km s^{-1}. The jet velocity derived here for AFGL 5142 MM1 is consistent with other values for MYSOs from the literature (Marti, Rodriguez & Reipurth 1995; Curiel et al. 2006; Guzmán et al. 2016; Rodríguez-Kamenetzky et al. 2016; Sanna et al. 2016).

4.1.4 Bowshock velocity gradient

As a closing remark on the observationally determined jet physical properties in AFGL 5142 MM1, we note a shallow yet well-structured velocity gradient across the NW bowshock masers (see Fig. A1). This could be interpreted as a flattened and expanding ejection or as rotation of the entrained material about the jet axis – a phenomenon widely sought in the context of massive star formation, as it would suggest that outflows are driven by magneto-centrifugal jets (see also Burns et al. 2015). Our data show that AFGL 5142 MM1 has potential as a target for future rotating jet investigations.

4.1.5 Combined VERA, VLBA and EVN view of AFGL 5142 MM1

AFGL 5142 has been observed by three different VLBI arrays: the VLBA (Goddi & Moscadelli 2006), the EVN (Goddi et al. 2007) and VERA (this work). These are presented together in Fig. 6.

The combined view of VLBI maser observations of AFGL 5142 depicts a prototypical disc–jet system: a structure ubiquitous in low-mass star formation and becoming increasingly encountered in MYSOs with well-studied cases including Orion Source I (Hirota et al. 2014), IRAS 20126+4104 (Moscadelli et al. 2011; Chen et al. 2016). Water masers trace a narrow episodic jet that emanates at an angle near perpendicular to the protostellar disc traced by 6.7 GHz methanol masers – a transition exclusive to MYSOs.

Downloaded from https://academic.oup.com/mnras/article-abstract/467/2/2367/2957034 by ASTRON user on 29 November 2018

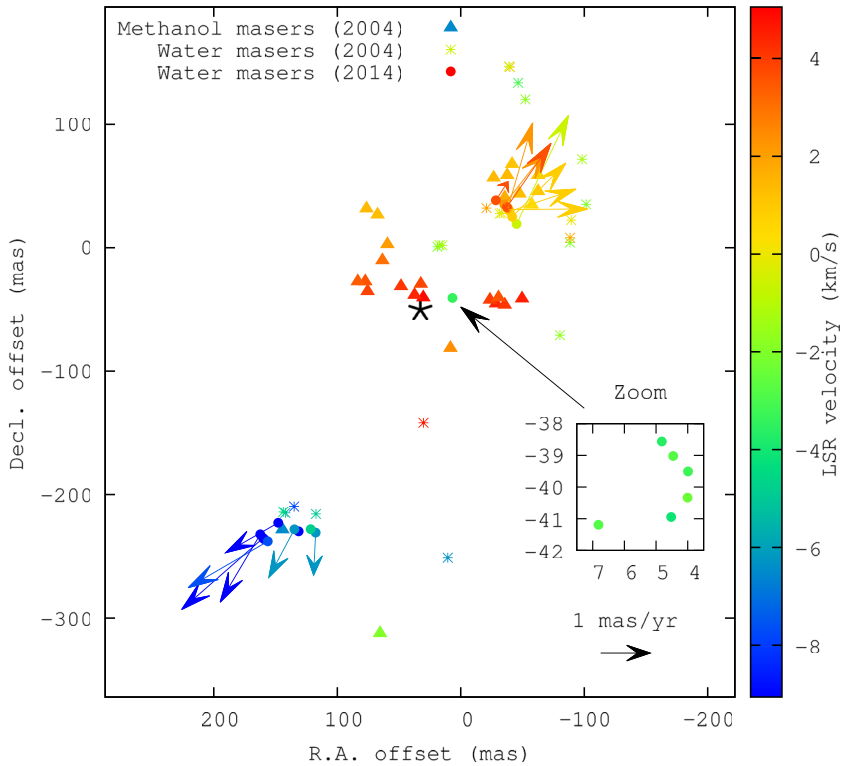

Figure 6. Combined view of 22-GHz water masers (filled circles) observed with VERA in 2010 (this work), 22-GHz water masers (asterisk) observed with the VLBA in 2004 (Goddi & Moscadelli 2006) and 6.7-GHz methanol masers (triangles) observed with the EVN in 2004 (Goddi et al. 2007). The inset shows the trajectory of maser feature A, moving in a clockwise fashion. The trajectory of feature A and proper motions of other masers are all converted to the YSO frame. The black asterisk symbol indicates the approximate origin of the episodic ejections, estimated from least-squares fitting of ellipses to the VERA maser data.

Maser feature A, detected in this work only, exhibits a curved trajectory and lies close to the likely position of the star as was inferred independently by the centre of kinematics of the 6.7-GHz methanol masers (Goddi et al. 2007), the centre of kinematics of the VLBA water masers (Goddi & Moscadelli 2006) and the concentric ellipses fit to VERA water masers, presented in Section 3.4. Non-linear motion implies the application of force – whether that be gravitationally or magnetically dominated, we expect that the maser must be in close proximity to the central object. The trajectory of feature A is shown in an inset in Fig. 6, where motion progresses from the upper right of the inset in a clockwise direction. The trajectory has been shifted to the frame of the star. We pursue a full decomposition of the trajectory of this maser in a future publication, targeting the central <100 AU region.

Overall, the features highlighted by the combination of VLBA, EVN and VERA observations reveal a system comprising a circumstellar disc from within which a narrow and collimated jet is launched. These features resemble those representative of low-mass YSOs. As we showed in Section 4.1.1, the outflow launching mechanism in AFGL 5142 MM1 also resembles those common to low-mass YSOs, while the outflow momentum rate of AFGL 5142 MM1 (Section 4.1.2) is larger than those typically seen in low-mass stars (Beuther et al. 2002). Episodic ejection, which in turn implies that accretion also occurs episodically, is another feature shared with low-mass disc-aided star formation. These points, taken together with the morphology and 3D kinematics of structures near the MYSO compiled from VLBI observations, reveal that AFGL 5142 MM1 depicts a 'scaled-up' picture of low-mass star formation.

4.2 Molecular outflows in the AFGL 5142 region

Previous attempts at locating the progenitors of the multiple outflows seen in AFGL 5142 struggled on account of there being more outflows (at least 4) than major millimetre cores (only two), and because most outflows intersect one or both of MM1 or MM2, we propose that several of the outflows in this region could be explained by episodic ejections from a slowly precessing outflow system. In a recent paper, Liu et al. (2016) consider that a precessing jet may be the best way to produce the EWBO that forms the subject of their investigation. We share this view and extend on justifications described as follows.

Outflows A and C from Zhang et al. (2007), the 'compact CO outflow' of Hunter et al. (1995) and the SiO and HCO^+ outflows of Hunter et al. (1999) share a trend, whereby the redshifted lobe of the outflow extends to the North, while the blueshifted lobes extend to the South. We evaluate this trend in Fig. 7 that shows the PA of the aforementioned outflows as a function of angular extent, which we take as analogous to the outflow age (more extended outflows are older). Given that the age of the more extended outflows are a few 10^4 yr old (Hunter et al. 1995, 1999), the precession has an approximate period of one revolution per 10^4–10^5 yr. For this analysis, we use only the northern, redshifted outflows since the southernly directed blueshifted outflows often appear to truncate near MM2, which is known to coincide with the densest part of the molecular envelope (see Fig. 4 of Zhang et al. 2007). Outflow details used in the analysis and references to the original works are given in Table 3.

Downloaded from https://academic.oup.com/mnras/article-abstract/467/2/2367/2957034 by ASTRON user on 29 November 2018

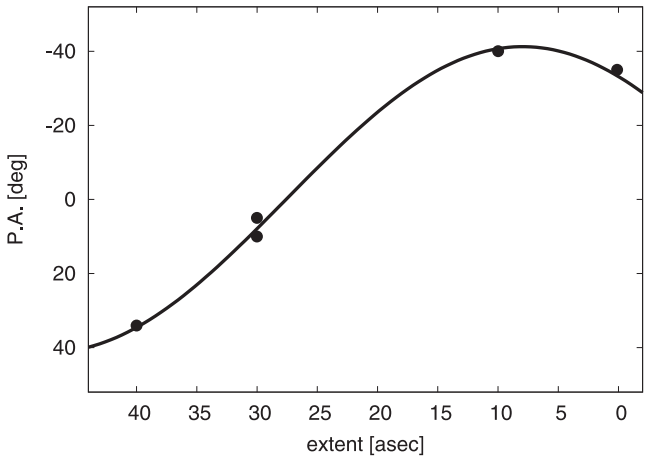

Figure 7. The angular extent of outflows from Table 3 as a function of position angle. A sinusoid represents expected values for a slowly precessing outflow, fit to the data.

Fig. 7 demonstrates the plausibility that the outflows listed above emanated from a single, precessing jet system, which we can confidently attribute to MM1 thanks to works at the highest angular resolution (Goddi & Moscadelli 2006; Goddi et al. 2011 and this work). To further test this hypothesis, we consider the momentum rates of each outflow, which we calculate or re-evaluate from the literature using our trigonometric distance of 2.14 kpc and record in column 4 of Table 3. All outflows under consideration have comparable momentum rates, supporting the hypothesis that they were driven by the same progenitor.

Regarding the remaining outflows, outflow D was likely driven by MM2 since its East-West orientation matches the central axis of the bowshock in the FS masers (Figs 8 and A2), and also the proper motions of the FS and FSE masers (Fig. 8). Note that both millimetre cores of MM1 and MM2 are elongated in the direction perpendicular to the assigned outflows, a known attribute of disc–jet systems (Reid et al. 2007).

The velocity orientation and position angle of outflow B is opposite to those of outflows A and C, ruling out an association with MM1. Outflow B may be driven by MM3 that could be a low-mass YSO (Zhang et al. 2007). MM3 sits between the blue- and red-shifted lobes of outflow B, where Zhang et al. (2007) detect weak 8.4 GHz continuum emission at the location of the millimetre core. The authors thus argue that MM3 may be of stellar nature, while the remaining millimetre cores MM6, MM7, MM8 and MM9 can be explained as dust condensations swept up by molecular outflows D, A/C, A and C, respectively.

4.3 Episodic ejection in AFGL 5142

Bowshocks trace the leading edges of new ejection events. As such, multiple bowshocks imply a history of multiple ejections. In Section 3.4, we present evidence of episodic ejection operating on time-scales of 10^1 yr, based on maser data. In Section 4.2, we argue that several of the molecular outflows in AFGL 5142 appear to stem from AFGL 5142 MM1. Regarding the dynamical time-scales of these molecular outflows, the older, more extended outflows from

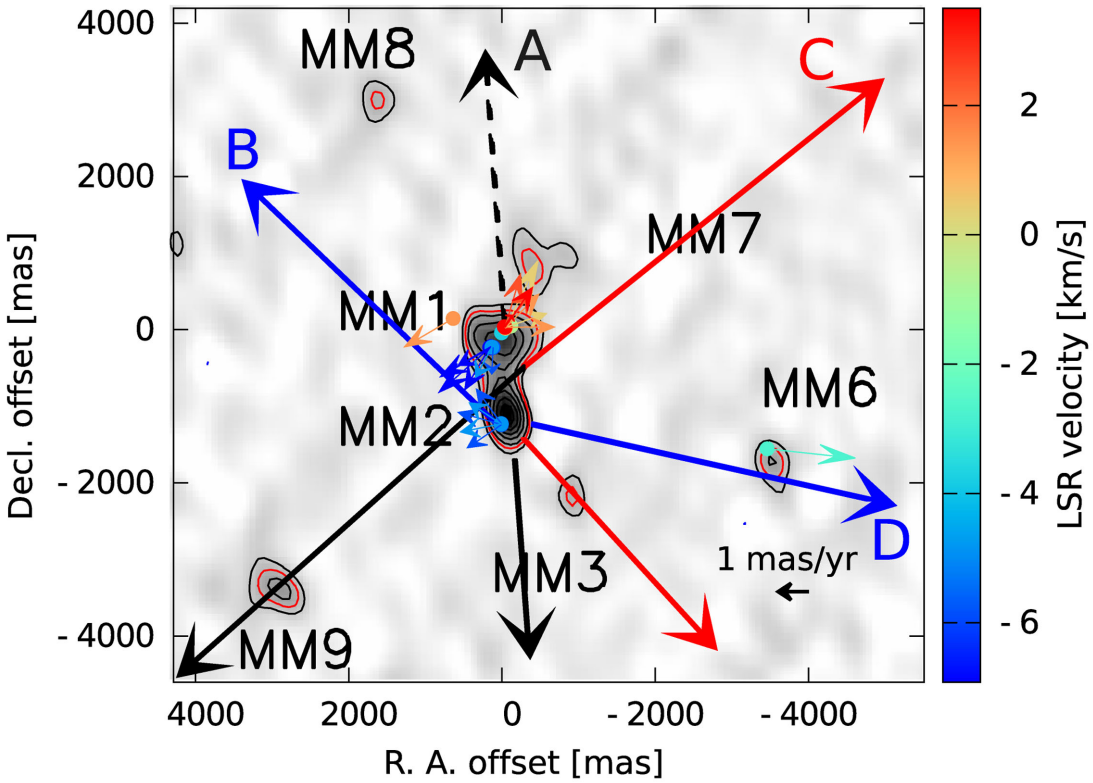

Figure 8. Overlay showing water maser activity in the context of the millimetre core and molecular outflows. Small arrow vectors are the same as in Fig. 2. Grey-scale shows the 1.3 mm continuum emission in the range of 0–0.07 mJy with contours at −4, 4, 8, 12, 16, 20 and 24 times the rms noise of 2.8 mJy beam^{-1}, from Palau et al. (2013), with the millimetre cores labelled. The red contour indicates the 6σ detection adopted by Palau et al. (2013). Larger arrows with letters annotated indicate the directions of molecular outflows described in previous works (Zhang et al. 2007; Palau et al. 2013).

Downloaded from https://academic.oup.com/mnras/article-abstract/467/2/2367/2957034 by ASTRON user on 29 November 2018

MM1 are a few 10^4 yr old (Hunter et al. 1995, 1999), while there are outflows associated with MM1 on four different scales (Table 3) – corresponding to ejection time-scales of every few 10^4 yr.

Since outflow activity is expected to correlate with accretion activity (Caratti o Garatti et al. 2015), the 10^4 yr time-scale of ejections could indicate alternating periods of accretion bursts and quiescence in AFGL 5142 MM1, consistent with time-scales predicted for episodic accretion in low- (Stamatellos, Whitworth & Hubber 2011) and high-mass stars (Meyer et al. 2017). The short episodic ejection seen on a 10-yr time-scales (Section 3.4) would likely originate in the inner disc.

The concept of episodic accretion is only recently being considered in the framework of massive star formation, though its ability to deal with the 'luminosity problem' and suppress the accretion inhibiting radiation field show great potential in explaining how massive stars accumulate their mass. AFGL 5142 presents a promising observational target for studies of episodic ejection and accretion in MYSOs.

5 CONCLUSIONS

Using VERA, a dual-beam VLBI array dedicated to astrometry, we measured an annual parallax for the AFGL 5142 massive star-forming region of $\pi = 0.467 \pm 0.010$ mas, corresponding to a trigonometric distance of $D = 2.14^{+0.051}_{-0.049}$ kpc.

Using the latest VLBI H_2O maser data, we analyse a recent ejection from the AFLG 5142 MM1 region that produced prototypical bipolar bowshocks that expand from a common centre in a circumstellar disc. We use the 3D kinematics of the maser bowshocks to investigate the physical properties of the protostellar jet.

One of the masers near the likely position of the star exhibits clear non-linear motion. The immediate region around the star requires further deep observations to provide vital context for this very unusual finding.

Combining our data with those of other published VLBI observations and through proper motion analysis, we find that AFGL 5142 MM1 is forming as a disc–jet system with evidence of episodic ejection, giving it the appearance of 'scaled-up' low-mass star formation.

Finally, we reinterpret the outflow history of AFGL 5142 MM1 as formation via an episodic, precessing outflow. We were able to suggest progenitor allocations for all outflows in AFLG 5142 known from the current literature.

ACKNOWLEDGEMENTS

RB would like to acknowledge the Ministry of Education, Culture, Sports, Science and Technology (MEXT) Japan for support as part of the Monbukagakusho scholarship.

We kindly thank the referee for providing helpful feedback and guidance during the review of this work.

REFERENCES

Beltrán M. T., Cesaroni R., Neri R., Codella C., Furuya R. S., Testi L., Olmi L., 2004, ApJ, 601, L187
Beuther H., Schilke P., Sridharan T. K., Menten K. M., Walmsley C. M., Wyrowski F., 2002, A&A, 383, 892
Burns R. A., Imai H., Handa T., Omodaka T., Nakagawa A., Nagayama T., Ueno Y., 2015, MNRAS, 453, 3163
Burns R. A., Handa T., Nagayama T., Sunada K., Omodaka T., 2016, MNRAS, 460, 283
Caratti o Garatti A., Stecklum B., Linz H., Garcia Lopez R., Sanna A., 2015, A&A, 573, A82
Chen H.-R. V., Keto E., Zhang Q., Sridharan T. K., Liu S.-Y., Su Y.-N., 2016, ApJ, 823, 125
Chernin L., Masson C., Gouveia dal Pino E. M., Benz W., 1994, ApJ, 426, 204
Chikada Y., Kawaguchi N., Inoue M., Morimoto M., Kobayashi H., Mattori S., 1991, in Hirabayashi H., Inoue M., Kobayashi H., eds, Frontiers of VLBI The VSOP Correlator. Universal Academy Press, Tokyo, p. 79
Corcoran M., Ray T. P., 1998, A&A, 331, 147
Curiel S. et al., 2006, ApJ, 638, 878
Goddi C., Moscadelli L., 2006, A&A, 447, 577
Goddi C., Moscadelli L., Sanna A., 2011, A&A, 535, L8
Goddi C., Moscadelli L., Sanna A., Cesaroni R., Minier V., 2007, A&A, 461, 1027
Guzmán A. E., Garay G., Rodríguez L. F., Contreras Y., Dougados C., Cabrit S., 2016, ApJ, 826, 208
Hartigan P., Morse J. A., Raymond J., 1994, ApJ, 436, 125
Hirota T., Kim M. K., Kurono Y., Honma M., 2014, ApJ, 782, L28
Hollenbach D., Elitzur M., McKee C. F., 2013, ApJ, 773, 70
Hunter T. R., Testi L., Taylor G. B., Tofani G., Felli M., Phillips T. G., 1995, A&A, 302, 249
Hunter T. R., Testi L., Zhang Q., Sridharan T. K., 1999, AJ, 118, 477
Ilee J. D., Cyganowski C. J., Nazari P., Hunter T. R., Brogan C. L., Forgan D. H., Zhang Q., 2016, MNRAS, 462, 4386
Imai H., Sakai N., Nakanishi H., Sakanoue H., Honma M., Miyaji T., 2012, PASJ, 64, 142
Kaufman M. J., Neufeld D. A., 1996, ApJ, 456, 250
Kawaguchi N., Sasao T., Manabe S., 2000, in Butcher H. R., ed., Proc. SPIE Conf. Ser. Vol. 4015, Radio Telescopes. SPIE, Bellingham, p. 544
Lee C.-F., Stone J. M., Ostriker E. C., Mundy L. G., 2001, ApJ, 557, 429
Liu T. et al., 2016, ApJ, 824, 31
Marti J., Rodriguez L. F., Reipurth B., 1995, ApJ, 449, 184
Meyer D. M.-A., Vorobyov E. I., Kuiper R., Kley W., 2017, MNRAS, 464, L90
Moscadelli L., Cesaroni R., Rioja M. J., Dodson R., Reid M. J., 2011, A&A, 526, A66
Ostriker E. C., Lee C.-F., Stone J. M., Mundy L. G., 2001, ApJ, 557, 443
Palau A. et al., 2011, ApJ, 743, L32
Palau A. et al., 2013, ApJ, 762, 120
Reid M. J., Menten K. M., Greenhill L. J., Chandler C. J., 2007, ApJ, 664, 950
Rodríguez-Kamenetzky A., Carrasco-González C., Araudo A., Torrelles J. M., Anglada G., Martí J., Rodríguez L. F., Valotto C., 2016, ApJ, 818, 27
Sanna A., Reid M. J., Carrasco-González C., Menten K. M., Brunthaler A., Moscadelli L., Rygl K. L. J., 2012, ApJ, 745, 191
Sanna A., Moscadelli L., Cesaroni R., Caratti o Garatti A., Goddi C., Carrasco-González C., 2016, A&A, 596, L2
Shepherd D. S., Yu K. C., Bally J., Testi L., 2000, ApJ, 535, 833
Stamatellos D., Whitworth A. P., Hubber D. A., 2011, ApJ, 730, 32
Tan J. C., Beltrán M. T., Caselli P., Fontani F., Fuente A., Krumholz M. R., McKee C. F., Stolte A., 2014, Protostars and Planets VI. Univ. Arizona Press, Tucson, p. 149
Wu Y., Wei Y., Zhao M., Shi Y., Yu W., Qin S., Huang M., 2004, A&A, 426, 503
Zhang Q., Hunter T. R., Beuther H., Sridharan T. K., Liu S.-Y., Su Y.-N., Chen H.-R., Chen Y., 2007, ApJ, 658, 1152
Zinnecker H., Yorke H. W., 2007, ARA&A, 45, 481

Downloaded from https://academic.oup.com/mnras/article-abstract/467/2/2367/2957034 by ASTRON user on 29 November 2018

APPENDIX A: VLBI IMAGES OF MASERS

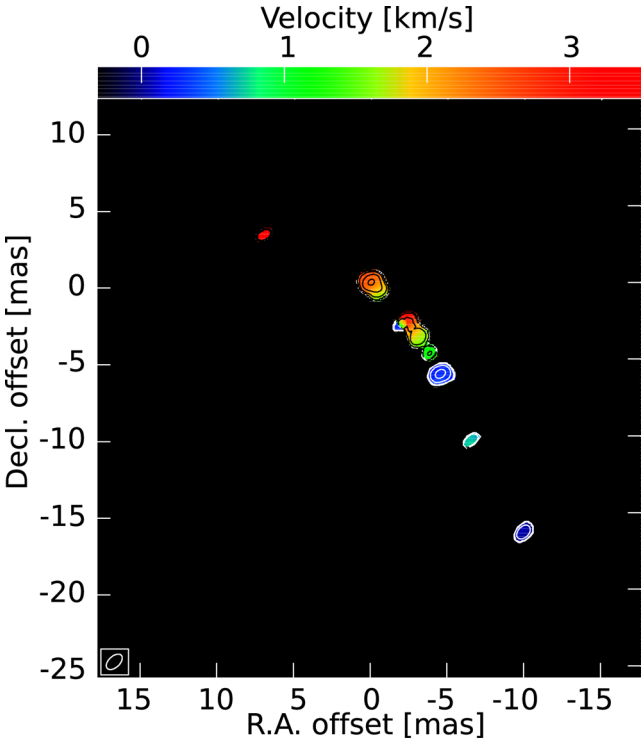

Figure A1. Maser distributions and l.o.s. velocities in the NW bowshock.

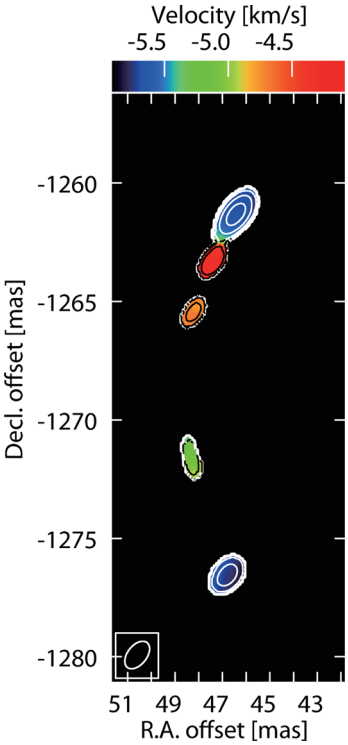

Figure A2. Maser distributions and l.o.s. velocities in the FS bowshock.

This paper has been typeset from a TEX/LATEX file prepared by the author.

Downloaded from https://academic.oup.com/mnras/article-abstract/467/2/2367/2957034 by ASTRON user on 29 November 2018